Electronic Supplementary Material (ESI) for Journal of Materials Chemistry A.
This journal is © The Royal Society of Chemistry 2023

Electronic Supplementary Information: How flat is the flatband potential?

Raphaël Poulain*,†,‡

†*Technical University of Darmstadt, Institute of Materials Science, Peter-Grünberg-Str. 2, 64287 Darmstadt, Germany.*

‡*UCLouvain, Faculty of Sciences, Place des Sciences 2 L6.06.01, 1348 Ottignies-Louvain-la-Neuve, Belgium.*

E-mail: p.raphael653@gmail.com

Contents

1 Experimental **S-3**

1.1 Sample preparation S-3

1.2 The DArmstadt's Integated SYstem for MATerial Science (DAISY-MAT) . . S-4

1.3 Hydrogen plasma treatment S-5

1.4 Interface and Bias assisted electron exposure experiments S-6

1.5 Electrical measurements S-8

1.5.1 Typical IV and EIS measurements S-8

1.5.2 Model and fits for the EIS measurements S-8

1.5.3 Thermionic voltage determination S-11

1.6 List of prepared samples and data extracted from the IV and EIS measurements S-14

2 PES profile simulation **S-15**

2.1 Introduction S-15

2.2 Si^0 simulation vs experiments S-16

Bibliography **S-18**

References **S-18**

1 Experimental

1.1 Sample preparation

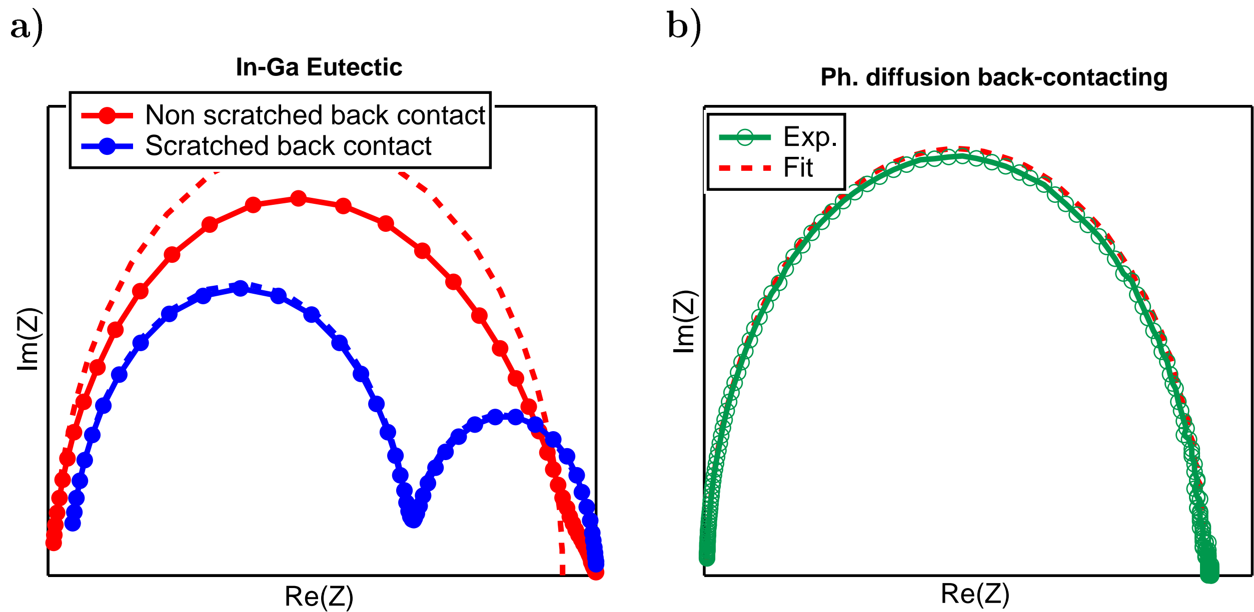

Figure S1: Nyquist representation of the electrochemical impedance spectroscopy (EIS) measurements obtained on a Si/SiO_2/Pt front contact with a) Indium-Gallium (In-Ga) eutectic as back-contact and b) with a phosphor doped n^+-rich back contact. The comparison of the measurements with a R//C model (see Section 1.5.2) evidences that the phosphor diffusion on the back-contact leads to a perfect single semi-circle, associated to the EIS pattern of the front contact, contrary to the sample with the In-Ga eutectic which produce non ideal semi-circles.

1.2 The DArmstadt's Integated SYstem for MATerial Science (DAISY-MAT)

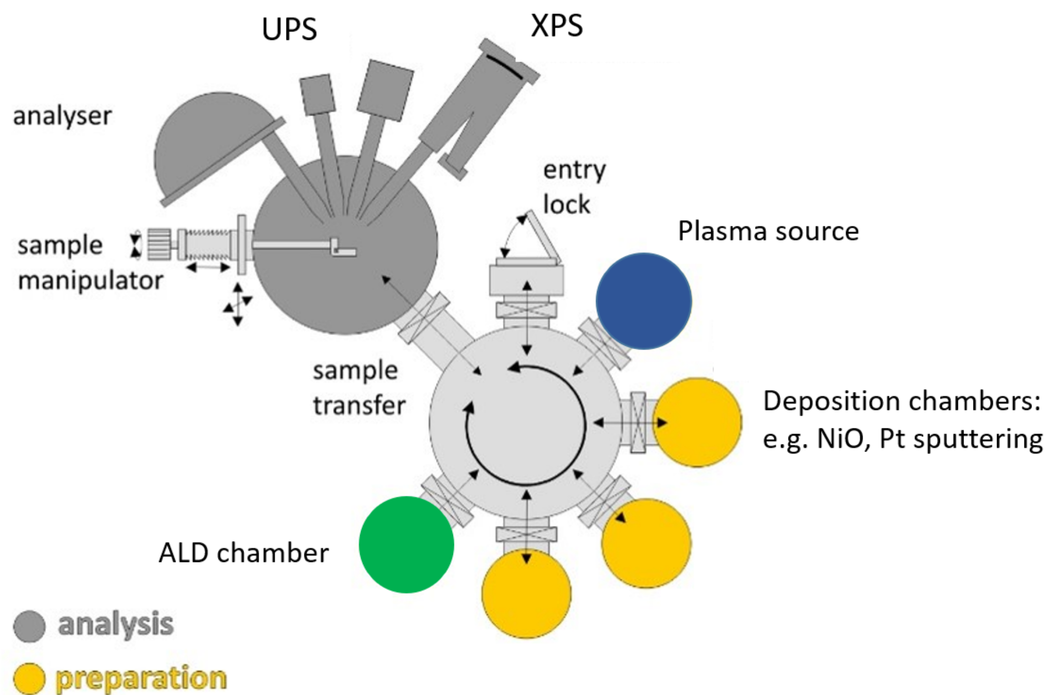

Figure S2: Schematic of the DArmstadt's Integated SYstem for MATerial Science (DAISY-MAT) system for the sample preparation and the in-situ photoelectron spectroscopy (PES) measurements.[S1]

1.3 Hydrogen plasma treatment

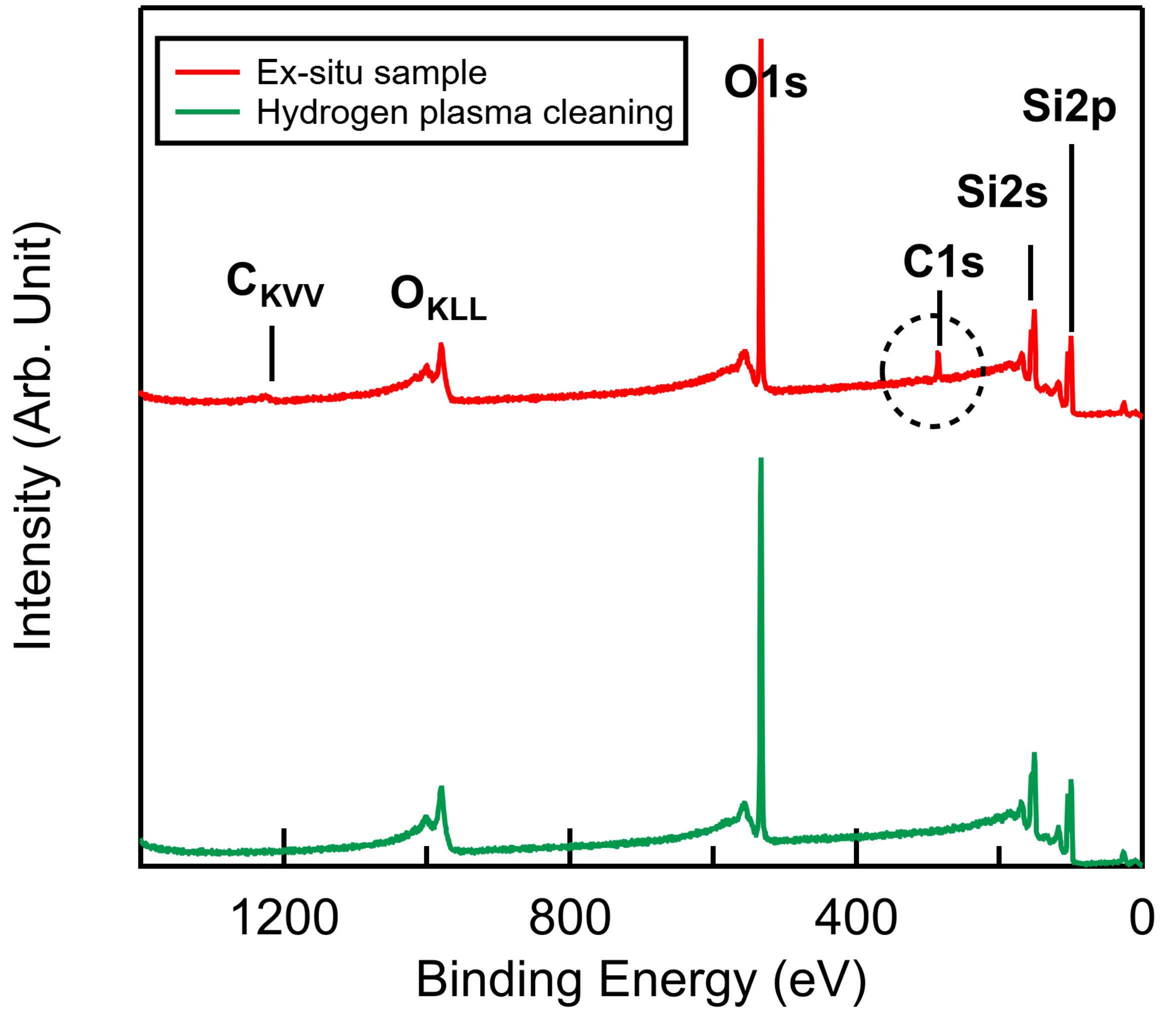

Figure S3: Survey PES measurements on ex-situ Si/SiO_2 and hydrogen plasma exposed Si/SiO_2 substrate. The carbon C 1s peak is totally removed after the hydrogen treatment.

1.4 Interface and Bias assisted electron exposure experiments

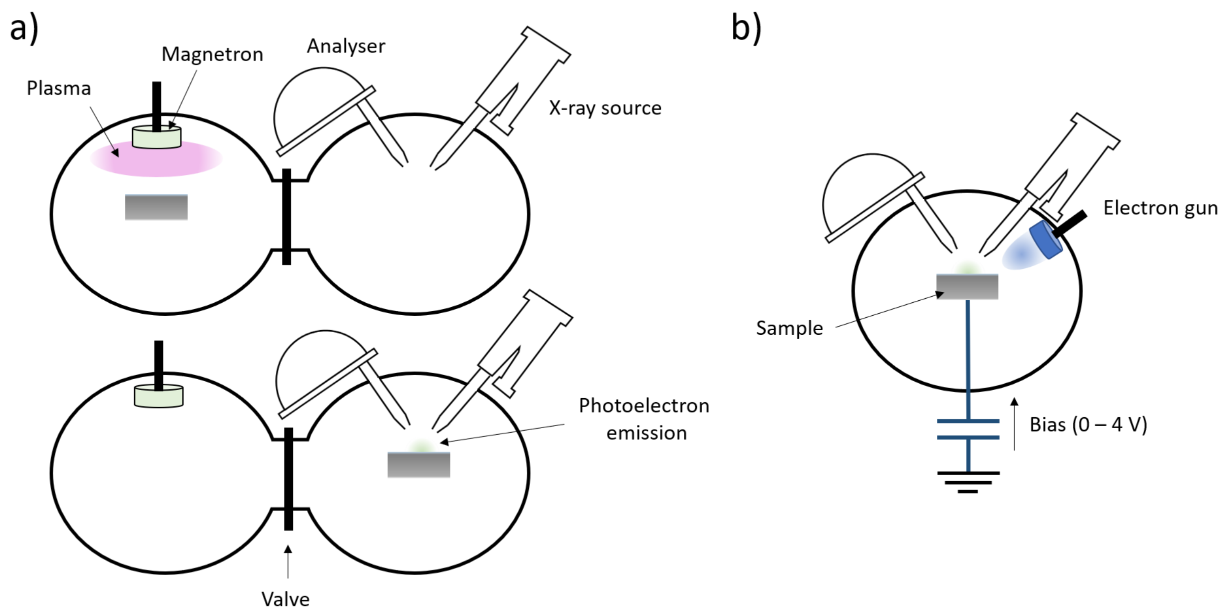

Figure S4: Schematic of the experimental setups adopted for the in-situ PES surface study of the hydrogen plasma treated Si/SiO_2 samples with a) the interface experiments where the spectra are recorded for an increment (< 1 nm) of deposited material in the sputtering chamber and b) the bias assisted electron exposure experiments where the samples are exposed to an electron flux during a positive potential bias.

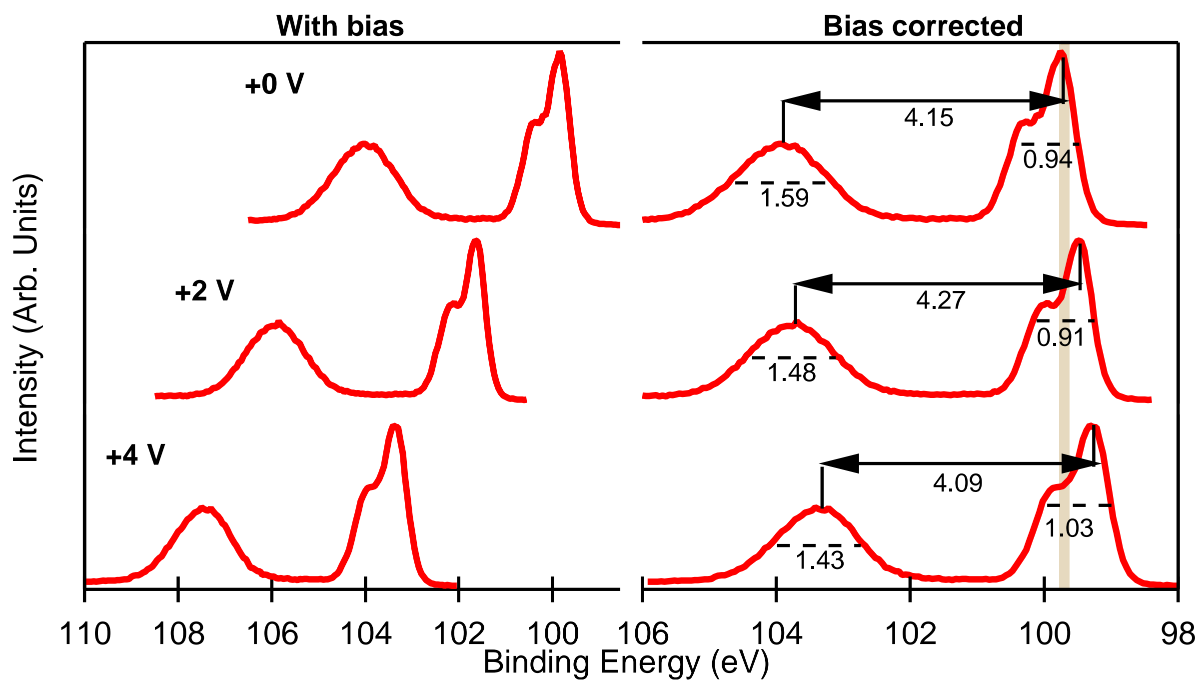

Figure S5: Left: Raw PES data collected in the Si 2p region during the bias assisted electron exposure experiments. Right: after bias potential correction.

1.5 Electrical measurements

1.5.1 Typical IV and EIS measurements

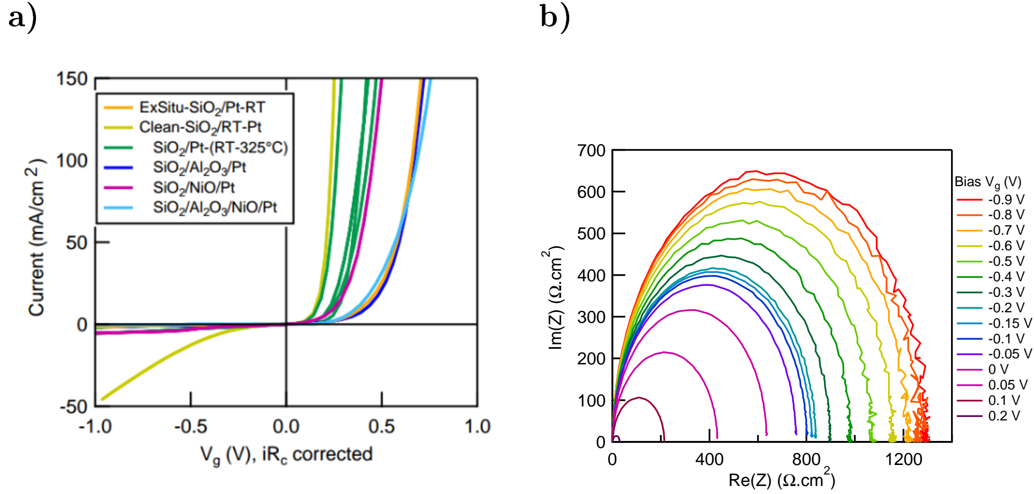

Figure S6: Typical a) current-voltage (IV) curves and b) Nyquist plot of the electrochemical impedance spectroscopy (EIS) data obtained with the Pt terminated Schottky structures with an Ohmic back contact obtained by phosphor diffusion as described in the experimental part of the manuscript. The IV curves and the EIS measurements displays a rectifying behavior and a semi-circle in reverse bias potential, respectively. These are typical features of diode like Schottky contact.

1.5.2 Model and fits for the EIS measurements

As displayed in Figure S6.b, the EIS measurements evidence the presence of semi-circles at any bias which is typical of resistive and capacitive elements connected in parallel (R//C). The fits of the EIS data were realized with an error value representing less than 0.1%.

After the EIS data analysis, three patterns can be observed according to the bias potential region: the reverse, the intermediate and the forward potential (see Figure S7).

At reverse bias (Figure S7.a), the Nyquist plot displays one semi-circle which can be easily fitted with a $R_c+R_{leak}//C_{scr}$ electrical equivalent circuit where R_c, R_{leak} and C_{scr} are the contact resistance, the leak resistance and the space-charge region capacitance, respectively.

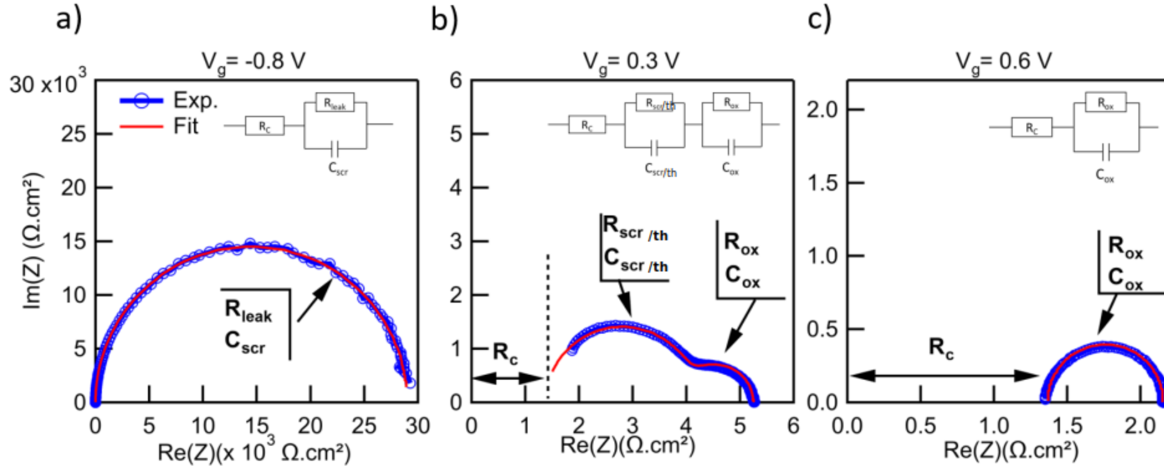

Figure S7: Typical electrochemical impedance spectroscopy (EIS) measurements on a hydrogen plasma treated Si/SiO_2/Pt front contact at a) reverse (V_g =-0.8 V), b) intermediate (V_g =0.3 V) and c) forward potential (V_g =0.6 V). The red line is the fit of the experimental data with an electrical equivalent circuit as represented in the inset.

Indeed, the analysis of the EIS data shows that in reverse bias, the current flowing through the leak resistance dominates (see Section 1.5.3) while the Mott-Schottky plot of the extracted capacitive element in this potential region displays a linear slope (see the Figure 2.c of the manuscript) from which the donor density (N_d) of the studied n-type silicon can be obtained. For this reason, the leak resistance is found in parallel to C_{scr} at reverse bias.

At intermediate potential (Figure S7.b), the Nyquist plot can display two semi-circles. In this potential region the EIS data are fitted with a R_c+($R_{scr/th}$//$C_{scr/th}$)+(R_{ox}//C_{ox}) with $R_{scr/th}$ and $C_{scr/th}$ the resistance and the capacitance element associated to the SCR or the thermionic current under small perturbations (see Equation 1) depending on the situation. Indeed, with increasing bias potential, the SCR becomes smaller and might even totally disappear at intermediate potential for the structure providing a negative V_{fb}. In the Section S1.5.3 it is shown that at intermediate potential the current can be controlled by thermionic exchange but not as much through the leak resistance which is rather potential independent. The intermediate potential can be a potential region expressing a transition in the

current control and it might be more difficult to determine what is the origin of the current flow. In addition, because of the quasi-absence of the SCR, the effect of the oxide layers can be measured leading to the measurement to an additional semi-circle. The oxide layer is characterized by a resistance R_{ox} and a capacitance C_{ox}. Also, it has been observed a third semi-circle in the intermediate potential for the SiO_2/NiO/Pt sample but this case is not investigated further in this study.

At forward potential the capacitive element associated to the SCR and/or the thermionic potential is eliminated and no capacitive element can be measured apart of the oxide layer (Figure S7.c).

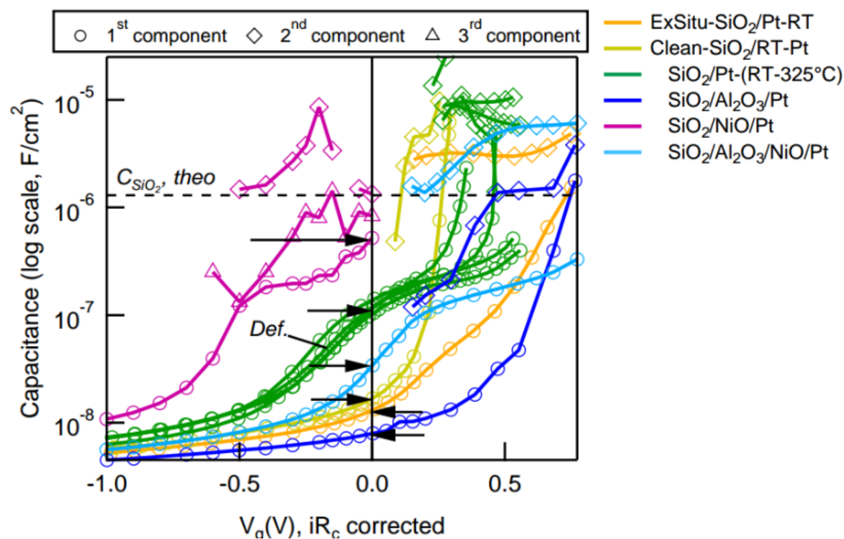

Figure S8: Capacitive elements extracted from the EIS measurements according to the bias potential, where the 1st, 2nd and 3rd elements are related to the number of R//C elements necessary to fit the experimental data in the Nyquist representation. The label *Def.* stands for defects and the horizontal arrows indicate the value of the C_{scr} used to determine V_{bi}.

The Figure S8 represents the extracted capacitive elements from the differently prepared Pt terminated Schottky contact. Three capacitive elements are evidenced in Figure S8: the 1st which is associated to the C_{SCR} and the $C_{SCR/th}$, the 2nd which is associated to the C_{ox} and the 3rd only visible for the SiO_2/NiO/Pt sample. The shape of the 1st capacitive element in

Figure S8 (see the label *Def.*) displays a bump for the structures delivering negative V_{fb}. This bump is assumed to originate from the ionization of the shallow defect under reverse potential. This bump is not visible for the structures providing the most positive V_{fb}. The 2nd capacitive element in forward bias ($\sim 5 \times 10^{-6}$ F/cm^2) is associated to the silicon dioxide layer (C_{SiO_2}). In theory the C_{SiO_2} value for a 2.5 nm SiO_2 layer is expected to be 1.3×10^{-6} F/cm^2 (horizontal line in Figure S8). Because of the reduction of the effective distance of the parallel plate capacitor model or tunneling effects for such thin layer the measured C_{ox} could be higher than the calculated one.

1.5.3 Thermionic voltage determination

Figure S6.a displays the current-voltage (IV) measurements of the fabricated Pt terminated Schottky junctions and evidence a rectifying behaviors of the fabricated device. The IV curves were used to extract j_0 and so the V_{th} values in the 0.1 to 0.4 V forward potential region after voltage correction with the contact resistance R_c determined by EIS. The ideal potential region for extracting j_0 and V_{th} have been determined when the charge transfer (the current) at the Schottky contact originates from a thermionic regime (diode regime) and not by other paths leading to parasitic current.

The resistance associated to the thermionic regime can be determined from the Equation 7 of the manuscript for small perturbations:

$$\frac{\partial I}{\partial V_g} = \frac{-q\, j_0}{\eta\, k_b T} * exp(-\frac{qV_g}{\eta\, k_b T}) = 1/\,\mathrm{R_{th}} \tag{1}$$

This equation suggests the presence of a linear slope $\frac{q}{\eta\, k_b T}$ in a log-scale which should indicate a thermionic regime. Figure S9.a shows the log scale plot of the inverse of the resistance R_{leak} and R_{scr} measured by EIS according to the bias potential V_g.

The plot Figure S9.a evidences that the expected linear behavior associated to the thermionic regime can be only visible at intermediate potential and more precisely between 0.1 to 0.4 V. In reverse potential, the current is mainly controlled by the potential-independent leakage resistance as it can be seen by the almost flat behavior of the curve. The analysis including the thermionic regime should not be confounded with the SCR. Indeed, the analysis realized in the manuscript shows that the V_{fb} can be negative while the V_{bi} can be close to 0 V but the thermionic regime region is identified for positive bias potential. It might suggest that the thermionic regime may be mainly driven by the surface potential induced by the shallow interfacial defects.

Thus, as represented in Figure S9.b, the exchange current j_0 has been systematically determined from the value of the intersection with the vertical axis of the linear extrapolation of the current where it has been estimated the thermionic regime dominates.

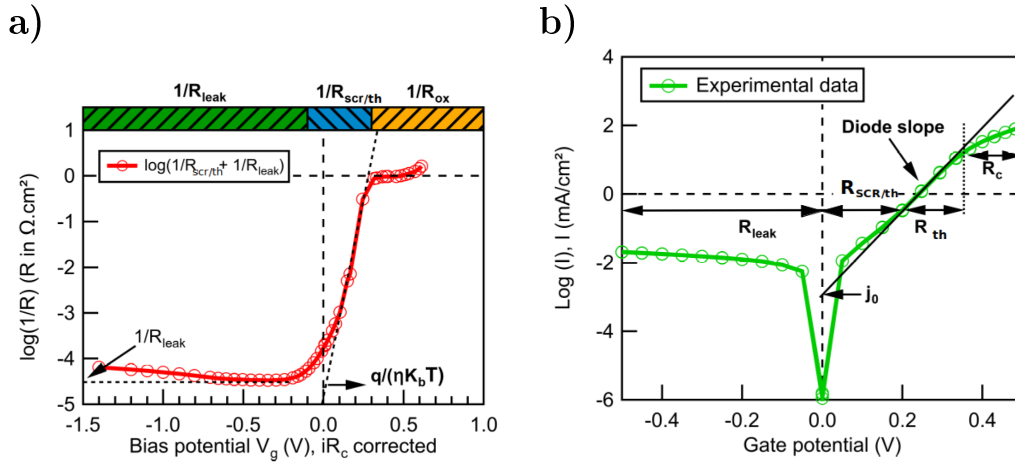

Figure S9: The plots describe the methodology for determining j_0. a) The analysis of the resistance measured by EIS evidence a linear region at intermediate potential associated to the evolution of the thermionic regime. Once the potential region is identified, b) the result is reported to the IV curves in log scale for which the linear extrapolation is used to determine the exchange current j_0.

It should be mentioned that the determination of the thermionic voltage V_{th} can be affected

by tunneling currents and the thicker the dielectric layer the higher V_{th} because of the reduction of the exchange current.[S2] However, the results displayed in Table S1 do not evidence a clear relationship between the dielectric thickness and V_{th}, and so it is assumed that the tunneling effect is in the same order of magnitude for each junctions produced in this study. However, with regards to the experimental setup, parasitic currents, such as leak currents, in the thermionic regime cannot be totally excluded and the derived V_{th} cannot be trusted with high confidence.

1.6 List of prepared samples and data extracted from the IV and EIS measurements

Table S1: List with all the Pt terminated Schottky samples realized for this study. The structure is related to the front contact fabricated on the n-Si(100) material. Ohmic back contact is obtained by phosphor diffusion as detailed in the experimental part of the manuscript and in the Section S1.1. The SiO_2 layer is about 2.5 nm and exposed to a plasma treatment as detailed in the experimental part of the manuscript, except for the ExSitu and Clean-SiO_2 which were untreated and exposed to a low temperature plasma treatment, respectively. Unless specified, the ALD-alumina layer is prepared with a first TMA pulse, for 10 cycles at 100 °C and are hydrogen plasma treated as detailed in the experimental part of the manuscript.

	j_0 (μA cm^{-2})	η_{IV}	V_{bi} (V)	V_{fb} (V)	V_{th} (V)
ExSitu-SiO_2/RT-Pt	12	1.7	0.202	0.19	0.41
Clean-SiO_2/RT-Pt	120	1.4	0.13	0.06	0.36
SiO_2/RT-Pt	169	2.3	0.002	-0.29	0.35
SiO_2/50°C-Pt	64	1.3	2.7×10^{-3}	-0.24	0.38
SiO_2/150°C-Pt	46	1.6	3.2×10^{-3}	-0.28	0.4
SiO_2/325°C-Pt	40	1.8	1.8×10^{-3}	-0.24	0.4
SiO_2/Al_2O_3/Pt	60	3.1	0.57	0.48	0.34
SiO_2/Al_2O_3(200°C,H2O 1st)/Pt	83	1.9	2×10^{-3}	-0.4	0.35
SiO_2/Al_2O_3(200°C)/Pt	43	2.3	2.6×10^{-3}	-0.35	0.37
SiO_2/Al_2O_3(5 cycles, RT)/Pt (3 A)	160	4.9	0.61	0.53	0.34
SiO_2/Al_2O_3(RT)/Pt (3 A)	79	2.6	0.33	0.28	0.36
SiO_2/Al_2O_3(RT)/Pt (3 A)	10	1.8	0.21	0.26	0.41
SiO_2/Al_2O_3(5 cycle, 100 °C)/Pt (3 A)	1.3	1.4	0.58	0.35	0.46
SiO_2/Al_2O_3/Pt (3 A)	70	2.7	6×10^{-2}	0.05	0.36
hp-SiO_2/Al_2O_3(100 °C)/Pt (3 A)	76	2.4	8.5×10^{-3}	-0.13	0.36
SiO_2/NiO/Pt	160	2.4	1.4×10^{-4}	-0.6	0.35
SiO_2/Al_2O_3/NiO/Pt	7	1.5	0.03	-0.03	0.43

2 PES profile simulation

2.1 Introduction

PES profile simulations have been performed in the Si 2p region for assessing the underlying surface potential profile near the Si/SiO_2 interface following the theory detailed in the manuscript. The models have been then compared to the observed experimental Si^0 and Si^{IV} peak distortion during the bias assisted electron exposure experiments and the interface experiments as represented in Figure 2.a and 2.b of the manuscript. The ideal PES peaks I_{id} have been reconstructed from the experimental peaks displaying a minimal width as it can suggest a minimal potential drop through the probed layer.

Therefore, the ideal Si^0 peak is the deconvolved Si^0 peak obtained during the bias assisted electron exposure experiments providing the smallest width (point 2 in Figure 2.a of the manuscript). As shown in Figure S10, the Si^0 peak is made of the Si 2p(1/2) and the Si 2p(3/2) spin orbits. An additional state (Si 2p Def.) accounting to defects in the silicon subsurface has to be also considered for realizing the fit. The Si 2p Def. state has not been further investigated but it can originate from hydrogen bonded to silicon (Si-H)[S3] or a surface/interfacial component.[S4,S5] Finally, the experimental data obtained at the point 2 of Figure 2.a of the manuscript have been fitted with three Gaussians-Lorentzian (ratio G/L=0.2) and a spin-orbit ratio of 0.5. The fit provided a spin orbit separation of 0.61 eV, close to the expectations[S3] while Si 2p Def. generates about 7 % of the total Si 2p peak intensity. The width at half maximum is 0.49 eV, 0.52 eV and 0.35 eV for the Si 2p(3/2), the Si 2p(1/2) and Si 2p Def., respectively. The ideal Si^0 PES peak (I_d) has been reconstructed accordingly to this fit.

Similarly, the smallest Si^{IV} width is being associated to a no-potential drop condition and is supposed to provide an ideal Si^{IV} PES peak for the simulation. This condition is met in

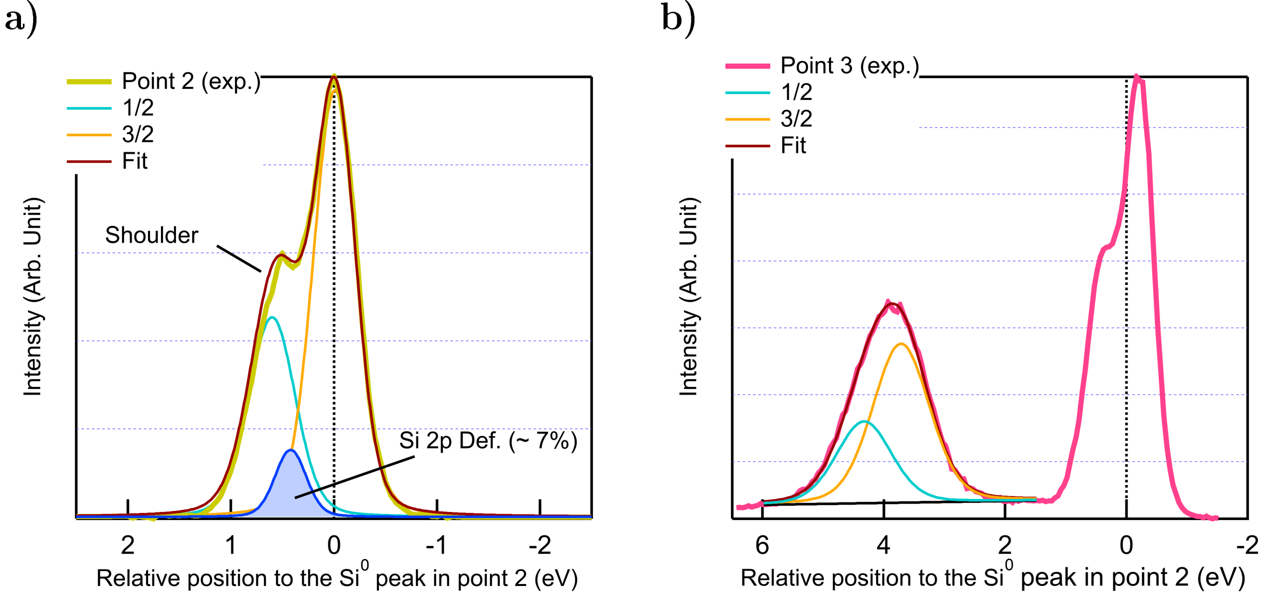

Figure S10: a) Deconvolved Si^0 spectra taken at the point 2 of Figure 2.a of the manuscript and b) Deconvolved Si^{IV} spectra taken at point 3 of Figure 2.a of the manuscript. The deconvolved spectra are the spectra providing a minimal width for the respective peaks as it is an indication of a minimal potential drop. Both spectra were recorded during the bias assisted electron exposure experiment. The origin of the horizontal axis is defined according to the position of the Si^0 peak in point 2 of the Figure 2.a of the manuscript.

point 3 of the Figure 2.b of the manuscript where the Si^{IV} peak width reaches a minimum of 1.41 eV. As shown in Figure S10.b, the Si^{IV} peak is deconvolved with voigt functions (ratio G/L=0.2) along a spin-orbit configuration with a 1/2 and a 3/2 components being distant of 0.61 eV. The relative ratio of the 1/2 and 3/2 areas is also set to 0.5 as for the Si^0 deconvolution. The width of each spin orbit is then estimated to 1.11 and 1.07 to the 1/2 and the 3/2 components, respectively. Contrary to the Si^0, the deconvolution of the Si^{IV} component can be satisfying without involving the presence of an intermediate state which can be associated to a defective states.

2.2 Si^0 simulation vs experiments

Simulated Si^0 peaks have been studied for potential profiles screening the top few nanometers (up to 7 nm) of the silicon subsurface from the Si/SiO_2 interface, as described in Figure 1.c

of the manuscript. As a primary parameter the Si^0 width at half maximum has been studied against its peak deviation as displayed in Figure 2.a of the manuscript. Thus, it has been found that an acceptable overlapping can be find if the top 5-6 nm of the silicon subsurface is screened by charges in the 10^{12} cm^{-2} range. For instance, a model with charges screening only the top 1.5 nm cannot account for the Si^0 peak deviation observed during the experiments. Indeed, as represented in Figure S11.a and S11.b, the simulated data misfit the Si^0 peak position of the experimental results obtained in point 1 and 3 of Figure 2.a of the manuscript with the 1.5 nm model. On the contrary, a 5 nm screened layer model provides a more satisfactory result as represented in Figure S11.c and .d. However, and very intriguing, the simulated Si^0 shoulder does not match the shoulder of the experimental Si^0 peak obtained in point 3 whereas the experimental and simulated spectra matches much more nicely in point 1.

Similar Si^0 shoulder mismatch could be observed if the Si^0 peak is measured during the interface experiments with Pt and NiO. More generally it is the case from the moment the Si^0 peak comes across the Fermi level pinning region in Figure 2.a when it shifts to lower binding energy.

After several iterations, it has been found that very likely the relative weight of the defective state evidenced in the deconvolution of the Si^0 measured in point 2 (see Figure S10.a) could vary in the course of the experiments. Indeed, PES simulated profile of the ideal Si^0 with 3.5 % Si 2p Def. of the defective state provides a more reasonable fitting with the experiments see Figure S11.d.

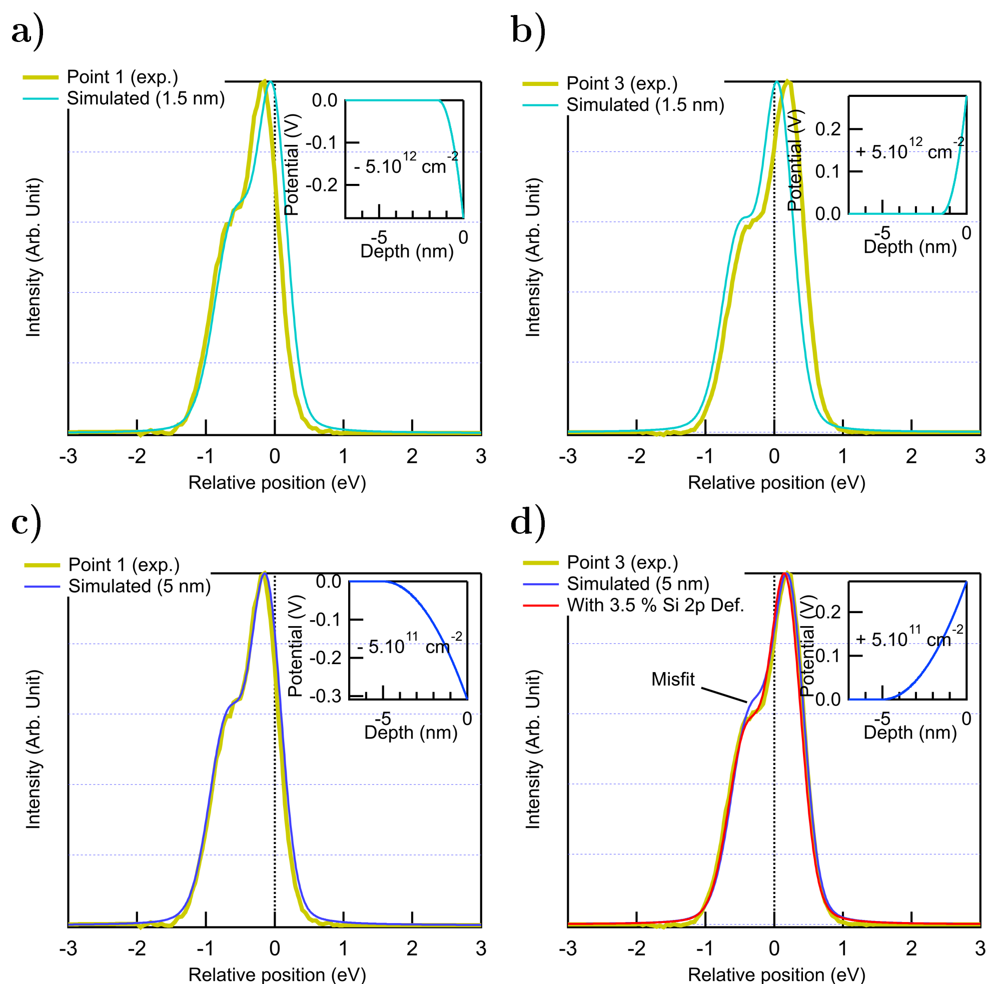

Figure S11: Comparison of the experimental point 1 and point 3 in Figure 2.a of the manuscript with the simulated Si^0 data for an underlying potential built-up in the silicon sub-surface generated by a negative and positive charges for a) and b) a screened layer of 1.5 nm and charge density $\pm$ 5.10^{12} cm^{-2} and c) and d) a screened layer of 5 nm and a charge density $\pm$ 5.10^{11} cm^{-2}. The PES profiles are plotted relatively to the Si^0 peak position in point 2 of Figure 2.a of the manuscript.

Bibliography

References

(S1) Klein, A. Transparent Conducting Oxides: Electronic Structure–Property Relationship from Photoelectron Spectroscopy with in situ Sample Preparation. *J. Am. Ceram. Soc.* **2013**, *96*, 331–345.

(S2) Hanselaer, P. L.; Vanmeirhaeghe, R. L.; Laflere, W. H.; Cardon, F. Large Barrier Tunnel Metal-Insulator - Semiconductor Structures. *Semiconductor Science and Technology* **1987**, *2*, 94–101.

(S3) Bjorkman, C. H.; Alay, J. L.; Nishimura, H.; Fukuda, M.; Yamazaki, T.; Hirose, M. Core-level shifts of silicon–hydrogen species on chemically treated Si surfaces studied by high-resolution x-ray photoelectron spectroscopy. *Applied Physics Letters* **1995**, *67*, 2049–2051.

(S4) Cricenti, A.; Ottaviani, C.; Comicioli, C.; Crotti, C.; Ferrari, L.; Quaresima, C.; Perfetti, P.; Le Lay, G. Sb-terminated Si(110), Si(100) and Si(111) surfaces studied with high resolution core-level spectroscopy. *Applied Surface Science* **2000**, *162-163*, 380–383.

(S5) Grupp, C.; Taleb-Ibrahimi, A. Core-level broadening mechanisms at silicon surfaces. *Journal of Electron Spectroscopy and Related Phenomena* **1999**, *101-103*, 309–313.